JCTC Journal of Chemical Theory and Computation

ARTICLE

pubs.acs.org/JCTC

TD-DFT Vibronic Couplings in Anthraquinones: From Basis Set and Functional Benchmarks to Applications for Industrial Dyes

Denis Jacquemin,*[,†] Eric Brémond,[‡] Aurélien Planchat,[†] Ilaria Ciofini,[‡] and Carlo Adamo*[,‡]

[†]Laboratoire CEISAM - UMR CNR 6230, Université de Nantes, 2 Rue de la Houssinière, BP 92208, 44322 Nantes Cedex 3, France

[‡]Ecole Nationale Supérieure de Chimie de Paris, Laboratoire LECIME, UMR CNRS-ENSCP no. 7575, 11, rue Pierre et Marie Curie, F-75321 Paris Cedex 05, France

Supporting Information

ABSTRACT: Vibrationally resolved absorption spectra of a series of anthraquinoidic dyes have been obtained with a polarizable continuum model time-dependent density functional theory approach. Firstly, we assessed the impact of the atomic basis set on both the transition energies and the vibronic shapes of 1,4-NH_2-anthraquinone using a large panel of Pople's basis sets, up to the 6-311++G(3df,3pd). In a second stage, an extensive functional benchmark has been performed to determine an adequate approach for the same compound. In the third step, a complete analysis of the origin of the band shape was performed for the same derivative. In the fourth stage, a set of functionals has been applied to investigate the position isomers in the dihydroxy anthraquinone series. Finally, in a last phase, the methodology has been used for three dyes of technological interest. It turns out that the chosen basis set has a relatively limited impact on the computed transition energies as well as the topology of the vibronic shape, but both are significantly influenced by the selected functional. In the present case, no single functional simultaneously provides highly accurate positions and intensities of the different bands, but ωB97XD appears to be a good compromise. This analysis allows to rationalize the difference in shapes experimentally noticed for the visible band of apparently similar anthraquinones.

1. INTRODUCTION

Commonly referred to as anthraquinone (AQ), 9,10-anthraquinone is composed of three fused aromatic rings, the central entity bearing two carbonyl groups (see Scheme 1). AQ derivatives are essential building blocks in several fields,[1−4] but the most common application of AQ compounds remains the dyeing of both natural and synthetic fibers. Indeed, substituted AQ may provide a complete and tunable panel of vivid colors if the auxochroms placed in positions 1−8 of the central core (see Scheme 1) are adequately selected.[5−10] Together with the existence of straightforward synthetic pathways and their thermal stability, the broad color palette explains why AQ dyes represent about one-fourth of today's organic world production of dyes.[6,8,11−18] The most simple anthraquinoidic dyes present an intense bell-shaped and structureless visible band, and the typical structure−property relationships used in color chemistry can be applied to adequately predict their absorption wavelength.[5] However, if two or more hydrogen-bond donors (typically alcohols or amines) are grafted in positions 1, 4, 5, or 8, strong interactions with the carbonyl groups play a key role and modify the properties of both the ground and the excited states. Consequently, the visible band of these AQ derivatives often features a characteristic multipeak structure.[5,7,8,13,19] The origin of multiple absorption maxima in quinoidic dyes is not necessarily unique, and proposals to explain this effect include aggregation,[20] tautomeric equilibrium,[21−23] and vibrational effects.[24,25] As we will demonstrate in this contribution, the latter explanation is by far the most appropriate for neutral AQ.

While there are numerous specific theoretical investigations aiming to simulate the absorption spectra of AQ dyes, only a few have focused on a large set of compounds in a way to obtain statistically relevant conclusions.[26−33] Without performing a detailed description of these previous studies, it turns out that time-dependent density functional theory (TD-DFT), within the popular vertical approximation is generally a (very) adequate tool to predict the λ_{max} of AQ derivatives but is obviously less accurate for the dyes presenting multiple absorption bands, e.g., the TD-DFT errors are larger for 1,4-NH_2-AQ (**I** in Scheme 1) than for 2-OH-AQ.[28] In this contribution, we aim to accurately simulate the absorption spectra of **I** as well as other challenging amino- and hydroxy-AQ presenting a structured visible band. To this end, we have to evaluate the vibronic couplings, in order to pinpoint one or more vibrational modes that hook up with the electronic transition and induce the experimentally observed specific shape of the visible band. To perform such task, one needs to calculate the Hessian of both the ground state and relevant (generally first) singlet excited state. While the first task is straightforward for molecules including a few dozen of atoms, the second job remains extremely challenging as the only available analytic method is the gas-phase configuration interaction singles (CIS) approach.[34] It is well-known that the quality of the CIS geometries for well-behaved excited states is comparable to its HF counterpart for the ground state, i.e., CIS is only sufficient if a qualitative picture is sought for.[35] In addition, CIS presents drawbacks to evaluate solvatochromic shifts.[36] To improve the accuracy of the simulations, one needs to include electron correlation. In practice, this can be done with TD-DFT. The first TD-DFT derivatives (gradients) allowing to

Received: April 15, 2011
Published: May 10, 2011

Scheme 1. Representation of the Systems Investigated Herein[a]

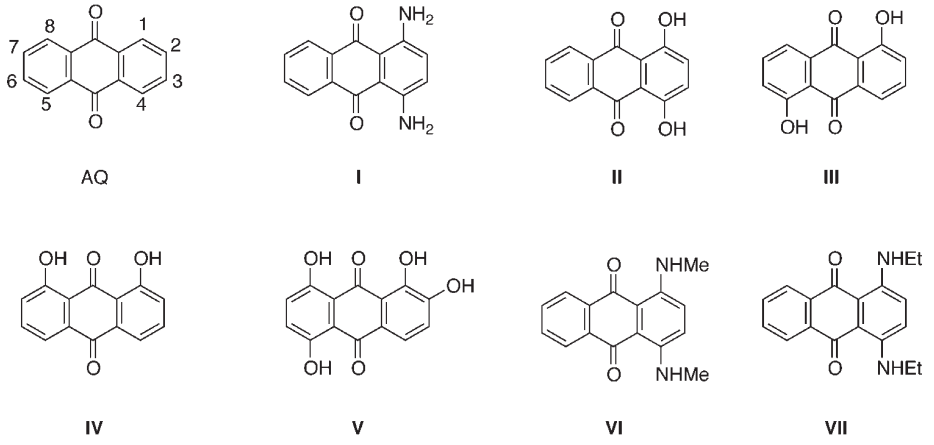

[a] For the generic anthraquinone (AQ), the numbering of substitution positions is also given.

Table 1. Basis Set Effects on the Ground and Excited-state of I.[a]

	ground state						excited state						vibronic			
basis set	PG	$d_{C=O}$	d_{C-N}	d_{Hbond}	λ_{vert} (f)	ZPVE	PG	$d_{C=O}$	d_{C-N}	d_{Hbond}	λ_{vert} (f)	ZPVE	ΔG	P_1^{conv} (I_r)	P_2^{conv} (I_r)	P_3^{conv} (I_r)
STO-3G	C_{2v}	1.312	1.360	1.280	527 (0.23)	6.10	C_s	1.310	1.397	1.372	667 (0.11)	6.08	2.12	517 (1.00)	429 (0.34)	367 (0.20)
6-31G	C_{2v}	1.273	1.356	1.791	520 (0.27)	5.97	C_{2v}	1.279	1.354	1.746	578 (0.26)	5.90	2.17	561 (1.00)	524 (0.61)	
6-31G(d)	C_s	1.242	1.354	1.822	516 (0.24)	5.87	C_s	1.249	1.348	1.761	590 (0.24)	5.80	2.13	561 (1.00)	527 (0.78)	
6-31+G(d)	C_s	1.245	1.353	1.828	521 (0.26)	5.83	C_{2v}	1.251	1.348	1.769	587 (0.26)	5.78	2.23	550 (0.92)	523 (1.00)	
6-31++G(d,p)	C_{2v}	1.245	1.352	1.813	521 (0.26)	5.83	C_{2v}	1.252	1.347	1.749	587 (0.26)	5.77	2.17	559 (1.00)	527 (0.88)	
6-31++G(2d,2p)	C_s	1.240	1.352	1.808	521 (0.25)	5.83	C_s	1.247	1.345	1.739	592 (0.24)	5.76	2.13	564 (1.00)	530 (0.79)	
6-311G(d)	C_s	1.237	1.351	1.844	520 (0.25)	5.84	C_{2v}	1.243	1.345	1.785	591 (0.24)	5.78	2.14	561 (1.00)	528 (0.85)	464 (0.18)
6-311+G(d)	C_s	1.238	1.352	1.845	518 (0.26)	5.83	C_s	1.245	1.347	1.786	589 (0.25)	5.77	2.12	561 (1.00)	527 (0.81)	
6-311++G(d,p)	C_s	1.238	1.352	1.823	519 (0.26)	5.81	C_s	1.246	1.347	1.758	592 (0.25)	5.75	2.15	562 (1.00)	528 (0.81)	
6-311+G(2d,p)	C_s	1.238	1.351	1.811	519 (0.25)	5.82	C_s	1.246	1.344	1.742	596 (0.24)	5.76	2.14	563 (1.00)	529 (0.82)	
6-311++G(2d,2p)	C_s	1.238	1.352	1.815	518 (0.25)	5.83	C_s	1.245	1.344	1.746	595 (0.24)	5.76	2.13	563 (1.00)	529 (0.82)	
6-311++G(2df,2pd)	C_{2v}	1.237	1.348	1.812	520 (0.25)	5.82	C_s	1.244	1.342	1.739	590 (0.25)	5.76	2.17	556 (1.00)	526 (0.97)	
6-311++G(3df,3pd)	C_{2v}	1.236	1.348	1.810	521 (0.25)	5.79	C_s	1.243	1.342	1.738	591 (0.24)	5.74	2.13	558 (1.00)	528 (0.94)	

[a] Point group (PG), selected distances (in Å), vertical transition energies (in nm) and zero-point vibrational energies (ZPVE in eV) are reported. The positions and relative intensities of the vibronic peaks (P_i^{conv}) obtained after convolution with a 0.05 eV fwhm Gaussian as well as the difference of Gibbs energies (ΔG, in eV) are also given. All results use a PCM(cychlohexane)-PBE0 approach.

optimize the excited-state geometries are available since the seminal work of van Caillie and Amos[37] and the subsequent extensions and improvements.[38−40] An extra advantage of TD-DFT, compared to more refined electron correlated wave function theories is the possibility to include bulk solvation effects during excited-state force minimizations, through the use of dielectric approximations, typically the polarizable continuum model (PCM).[40,41] Though PCM-TD-DFT vibronic simulations are becoming more and more popular,[25,42−50] they remain at the border of today's computational possibilities, as a numerical differentiation of the gradients is a prerequisite to obtain the excited-state Hessian, and therefore to simulate the vibronic spectrum. Therefore, PCM-TD-DFT calculations are generally applied to relatively compact (or symmetric) molecules using a predefined approach (basis set/functional) in order to limit the computational burden. For the first time, we tackle the vibronic spectra of AQ dyes, and we start with a complete benchmark work. In this framework, we have to highlight the key work of Dierksen and Grimme,[39] who computed (in the gas phase) the structured bands of a large set of molecules, principally fused aromatic, using three functionals. To the best of our knowledge, this 2004 paper that concluded that ca. 30−50% of exact exchange was optimal to reproduce experimental band shapes stands as the most complete vibronic benchmark to date.

This paper is organized as follows. In Section 2, we describe our computational protocol. In Sections 3.1 and 3.2, we investigate the basis set and functionals effects for **I**. Section 3.3 provides an in-depth analysis for this specific dye, whereas Section 3.4 gives the vibronic spectra of three dihydroxy AQ. In Section 3.5, we report vibrationally resolved spectra for selected "real-life" dyes, and eventually, we conclude.

2. METHOD

All our calculations have been performed with the Gaussian09[51] program, using default thresholds and algorithms except when noted. We have selected a large set of atomic basis

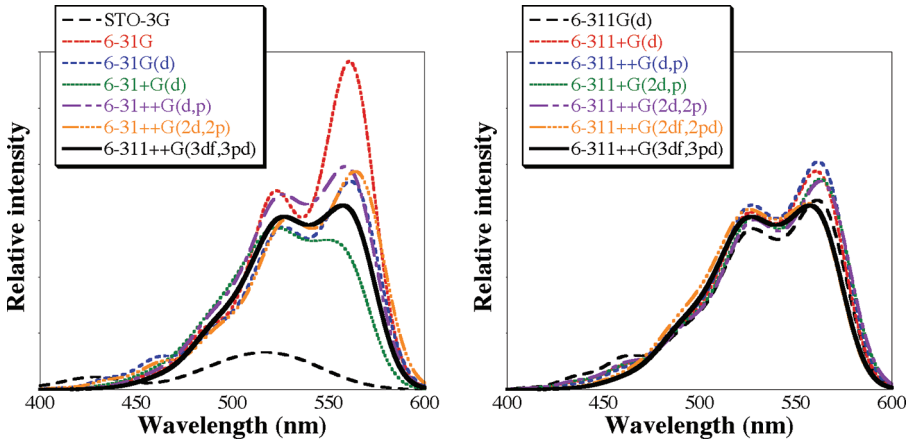

Figure 1. Comparison of the obtained vibronic shapes for system **I** using double-ζ (left) and triple-ζ (right) basis sets. In both cases, the reference 6-311++G(3df,3pd) black curve appears in bold.

sets (ABS) and DFT functionals: SVWN5,[52,53] BLYP,[54,55] PBE,[56] τ-HCTH,[57] O3LYP,[58] B3LYP,[59,60] X3LYP,[61] PBE0,[62,63] M06,[64] BMK,[65] BHHLYP,[66] M06-2X,[67] M06-HF,[64] CAM-B3LYP,[68] LC-PBE,[69,70] ωB97,[71] ωB97X,[71] and ωB97XD[72] to perform benchmarks for **I**, and we redirect the reader to these original references for complete description of these functionals. Though we have used the popular Pople's ABS in this paper, other possibilities, such as Jensen *pc*−*n*[73] ABS could have been selected as well. The ground-state (excited-state) geometries have first been optimized with DFT (TD-DFT) until the residual mean square forces are smaller than 1×10^{-5} au (tight threshold). Next, the vibrational frequencies have been computed analytically (numerically) for the S_0 (S_1) state. They confirmed the presence of minima characterized by the absence of imaginary modes (and transition states characterized by a single imaginary mode). In several cases, we have performed both force and frequency calculations using two or three point groups (PG) in order to ascertain the symmetry of all states. During all calculation steps, we have included bulk solvent effects by using the PCM[41] that correctly models the major solvent effects as long as no specific solute−solvent interactions are implied. Several solvents have been used (see below), but we have mainly selected an aprotic apolar solvent, so that the selection of the PCM model is fully legitimate. Vibrationally resolved spectra within the harmonic approximation were computed using the FCclasses program.[42,44,45] The reported spectra have been simulated at 298.15 K using a convoluting Gaussian functions presenting a full width at half-maximum (fwhm) of 0.05 eV during benchmark investigations. In other cases, the fwhm was adjusted according to the available experimental data as in ref 39. A maximal number of 25 overtones for each mode and 20 combination bands on each pair of modes were included in the calculation. The maximum number of integrals to be computed for each class was set to 1×10^6.

3. RESULTS AND DISCUSSION

3.1. Basis Set Investigation. For **I**, the results of the ABS investigation can be found in Table 1, whereas Figure 1 compares the corresponding vibronic shapes.[74] Separate representations of the stick and convoluted spectra, using a tighter Gaussian for convolution, can be found in the Supporting Information. We have used an uniform PCM-PBE0 method since global hybrids, and more specifically B3LYP and PBE0, have been found efficient within the vertical PCM-TD-DFT approximation for AQ dyes.[27,28] To the best of our knowledge, there are no previous investigations aiming at assessing the influence of the size of the chosen ABS on the shape of the vibronic bands of real-life molecules. This is certainly understandable, because computing numerically the vibrational TD-DFT spectrum is a very demanding task (several months of CPU for the largest ABS used here). Therefore, most TD-DFT benchmarks available in the literature[31−33,75−83] have been performed in the vertical model, whereas the studies also optimizing the excited-state geometries performed by Grimme and co-workers used a given basis set,[39,78,82] typically TZVP, a diffuseless triple-ζ ABS to determine the geometrical and vibrational parameters.

As can be seen in Table 1, the point groups of the ground and excited states are affected by the chosen ABS, the amino groups being perfectly coplanar to the AQ core (C_{2v}) or not (C_s). In the X-ray diffraction (XRD) structure[84] available for the dihydrate form of **I**, the amine groups are almost fully flat (torsion angles of ca. 2−3°), but they interact with water molecules, making straightforward comparisons with our cyclohexane simulations uneasy. In the XRD structure we obtained (see the cif file in Supporting Information and discussion below), the deviation of the amino groups is also trifling (ca. 4°). The energetic variations related to this change of PG are however limited, e.g., for 6-31G(d), the C_{2v} structures are, respectively, only 0.2 and 1.0 kcal·mol^{-1} less stable than the true C_s minima for the S_0 and S_1 states. In that sense, the obtained PG is probably not the most important discriminating factor. For **I**, it is striking that the ABS effects on the spectral properties are quite limited, as all selected Pople's basis leads to similar results, except for the two smallest that lack polarization functions. Even the compact 6-31G(d) provides vertical transition wavelengths and positions of the vibronic bands within 5 nm of the results obtained with 6-311++G(3df,3pd). The zero-point vibrational energy (ZPVE) computed for the ground and excited states are also nearly ABS independent, and the same holds for the small ZPVE decrease (ca. 0.05 eV) related to the $S_0 \rightarrow S_1$ transition. These findings may probably be quite specific to AQ dyes,[27] and we do not advocate to systematically use 6-31G(d) for TD-DFT calculations. As expected, the most sensitive geometrical parameter is the hydrogen bond (H-bond) distance between the carbonyl and the amine, that is significantly shortened when diffuse functions are added on both carbon and hydrogen atoms.

Table 2. Functional Benchmarks Obtained Using System I[a]

	ground state						excited state						vibronic			
functional	PG	$d_{C=O}$	d_{C-N}	d_{Hbond}	λ_{vert} (f)	ZPVE	PG	$d_{C=O}$	d_{C-N}	d_{Hbond}	λ_{vert} (f)	ZPVE	ΔG	P_1^{conv} (I_r)	P_2^{conv} (I_r)	P_3^{conv} (I_r)
SVWN5	C_{2v}	1.264	1.343	1.630	611 (0.21)	5.65	C_s	1.267	1.346	1.602	670 (0.18)	5.57	1.85	650 (1.00)	520 (0.09)	449 (0.00)
BLYP	C_{2v}	1.271	1.369	1.813	617 (0.20)	5.59	C_s	1.273	1.375	1.790	698 (0.17)	5.53	1.85	653 (1.00)	524 (0.21)	439 (0.01)
PBE	C_{2v}	1.267	1.360	1.769	614 (0.20)	5.62	C_s	1.270	1.367	1.741	692 (0.17)	5.56	1.87	647 (1.00)	518 (0.21)	439 (0.01)
τ-HCTH	C_{2v}	1.257	1.353	1.770	605 (0.21)	5.68	C_{2v}	1.260	1.359	1.743	681 (0.18)	5.63	1.92	638 (1.00)	511 (0.25)	428 (0.02)
O3LYP	C_s	1.250	1.357	1.836	561 (0.22)	5.76	C_s	1.254	1.359	1.803	646 (0.20)	5.71	2.06	592 (1.00)		
B3LYP	C_{2v}	1.251	1.360	1.835	536 (0.25)	5.77	C_{2v}	1.257	1.356	1.781	603 (0.25)	5.71	2.12	573 (1.00)	543 (0.95)	
X3LYP	C_{2v}	1.250	1.359	1.834	531 (0.25)	5.78	C_{2v}	1.257	1.354	1.778	598 (0.25)	5.73	2.14	568 (1.00)	537 (0.95)	
PBE0	C_{2v}	1.245	1.352	1.813	521 (0.26)	5.83	C_{2v}	1.252	1.347	1.749	587 (0.26)	5.77	2.17	559 (1.00)	527 (0.88)	
M06	C_s	1.242	1.357	1.850	514 (0.26)	5.78	C_{2v}	1.250	1.351	1.793	584 (0.26)	5.73	2.23	548 (0.98)	520 (1.00)	
BMK	C_{2v}	1.236	1.358	1.884	482 (0.29)	5.85	C_{2v}	1.246	1.348	1.801	558 (0.28)	5.79	2.37	491 (1.00)		
BHHLYP	C_s	1.230	1.356	1.870	445 (0.32)	6.02	C_{2v}	1.244	1.339	1.773	529 (0.31)	5.96	2.48	487 (0.84)	461 (1.00)	
M06-2X	C_s	1.236	1.360	1.888	465 (0.29)	5.84	C_{2v}	1.250	1.345	1.782	548 (0.29)	5.77	2.36	508 (0.89)	482 (1.00)	
M06-HF	C_{2v}	1.227	1.358	1.881	415 (0.34)	5.87	C_{2v}	1.252	1.331	1.669	538 (0.32)	5.77	2.56	443 (1.00)		
CAM-B3LYP	C_{2v}	1.241	1.357	1.844	470 (0.31)	5.85	C_{2v}	1.254	1.345	1.749	549 (0.30)	5.81	2.43	477 (1.00)		
ωB97	C_s	1.239	1.367	1.891	421 (0.34)	5.89	C_{2v}	1.256	1.345	1.771	520 (0.32)	5.83	2.57	441 (1.00)		
ωB97X	C_s	1.238	1.362	1.876	438 (0.33)	5.89	C_{2v}	1.253	1.344	1.764	527 (0.32)	5.83	2.52	454 (1.00)		
ωB97XD	C_s	1.240	1.359	1.856	467 (0.31)	5.86	C_{2v}	1.252	1.346	1.758	546 (0.30)	5.81	2.39	505 (0.90)	479 (1.00)	
LC-PBE	C_{2v}	1.229	1.347	1.817	415 (0.36)	5.97	C_{2v}	1.246	1.328	1.673	514 (0.34)	5.93	2.65	431 (1.00)		

[a] All results use a PCM(cychlohexane)-(TD-)DFT/6-31++G(d,p) level of theory, see Table 1 for more details.

For the carbonyl bond, going from a double-ζ to a triple-ζ ABS decreases its length by ca. 0.01 Å, but this effect is constant for both S_0 and S_1 states. At the exception of the 6-31+G(d), all double-ζ and triple-ζ basis sets predict that the longest wavelength peak is slightly more intense than its short-wavelength counterpart. As a compromise ABS in the following, we have selected 6-31++G(d,p) that presents both polarization and diffuse orbitals on all atoms and delivers relative intensities for the vibronic bands relatively close to the 6-311++G(3df,3pd) reference. Of course other basis sets, e.g., 6-311+G(d), could have been reasonable choices.

3.2. Functional Benchmark. The results obtained for 18 functionals are summarized in Table 2, whereas representations of the vibronic shapes may be found in Figure 2 as well as in the Supporting Information. Obviously, the selected functional impacts significantly on the computed $S_0 \rightarrow S_1$ ΔG and the corresponding transition energies, that tend to increase when more exact exchange is plugged in an expected trend for $\pi-\pi^*$ transitions (see previous benchmarks).[31,32,39,77,82] The predicted elongation of the carbonyl group upon electronic transition is also dependent on the DFT/HF blend, as it tends to increase when larger shares of exact exchange are applied. Even more striking are the evolutions of the C−N and H-bond distances induced by photon absorption. The former lengthens with the four pure functionals and O3LYP but shortens with all other functionals, an effect that is much larger with M06-HF (−0.027 Å) or LC-PBE (−0.019 Å) than with B3LYP (−0.004 Å). The H-bond distance is smaller in the S_1 than S_0 state but with a variation that is not a simple function of the exact exchange mixing parameter(s).

In ref 82, the authors have computed the geometries (and hence the ZPVE energies) at the PBE/TZVP level but selected a much larger basis set and a wide panel of functionals for determining the vertical transition energies. It is indeed common to use a given geometry and to benchmark the transition energies, a procedure that we have also used several times,[32,33,83,85] as the geometry optimization process may be time-consuming. For the ZPVE, the results listed in Table 2 justify such an approach: the PBE $S_0 \rightarrow S_1$ ZPVE shift is −0.08 eV, whereas B3LYP and ωB97XD estimates are relatively close, −0.06 and −0.05 eV, respectively. Therefore the implied error is negligible. For the vertical transitions, the impact of using a given geometry is apparently larger. Indeed, the vertical B3LYP and ωB97XD absorption wavelengths computed using the PBE ground-state structure are 554 and 502 nm, respectively, implying variations of −0.08 and −0.19 eV compared to the corresponding data calculated with a consistent structure (536 and 467 nm, see Table 2). The ωB97XD λ_{vert} computed on the B3LYP geometry is 482 nm, closer to the 467 nm reference value, but still implying a −0.08 eV deviation, that we recently neglected.[83] This is just one more illustration that the exact benchmark procedure could slightly tune the results and that such an outcome is inherent to all computationally tractable processes.

In the most recent experimental measurements,[13] the visible absorption band has been found to present three peaks in cyclohexane: 578.4, 567.2, and 537.6 nm with a shoulder (sh) at ∼500 nm.[13] The relative intensities are estimated to be 0.82, 0.82, 1.00, and 0.61 for the three peaks and the shoulder, respectively.[13] In dioxan, the first two bands are not distinguishable, and Perkampus reports in his famous book: 585 (0.92), 547 (1.00), and 510 nm (sh, 0.59).[9] The same holds in the protic and more polar solvant, ethanol: 592 (1.00), 551 (1.00) and 522 nm (sh, 0.81).[86] Obviously, the visible spectra provided by pure functionals (SVWN5, BLYP, PBE, and τ-HCTCH) and by approaches including a very large ratio of exact exchange (M06-HF, ωB97, and LC-PBE) are not satisfying neither for the predicted shapes nor for the transition energies. Hybrids including 15−30% of exact exchange yield accurate positions for the different bands but incorrectly predict a more

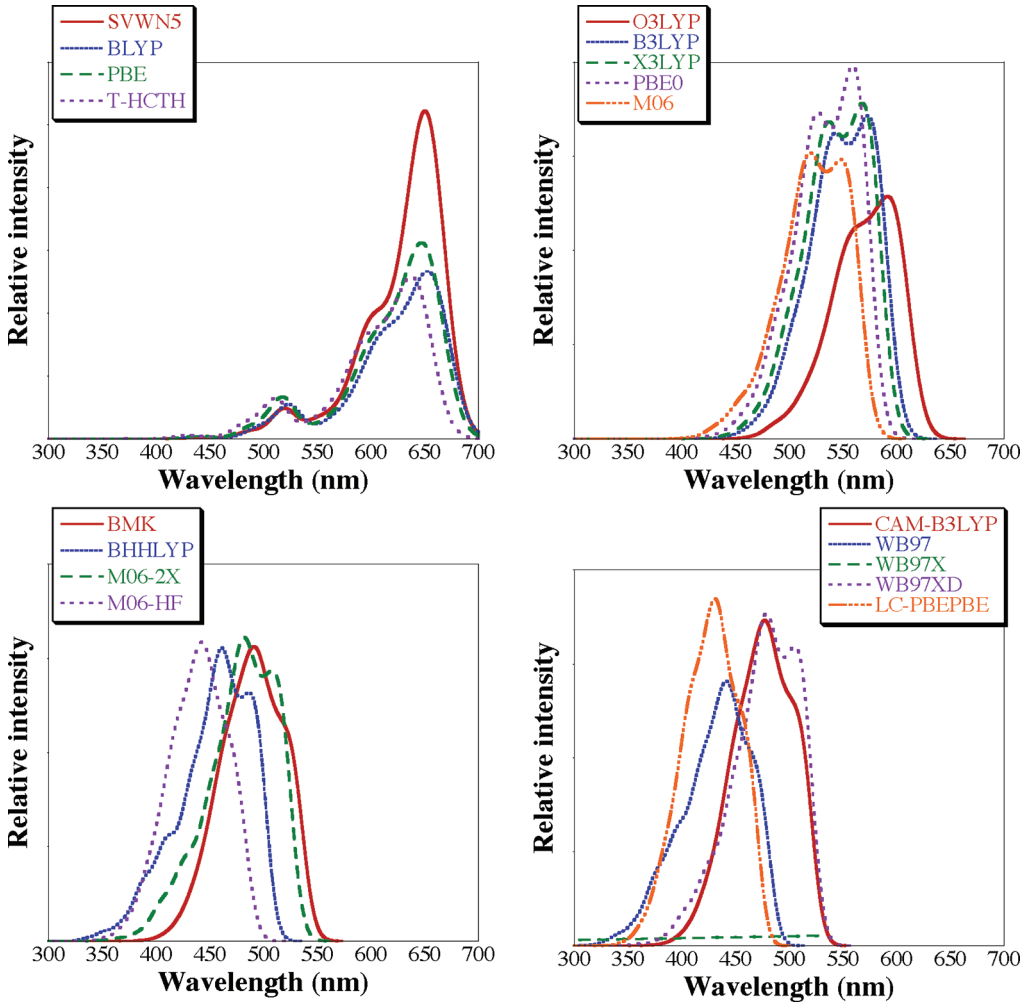

Figure 2. Comparison of the obtained vibronic shapes for system **I** using different DFT functionals and a PCM-TD-DFT/6-31++G(d,p) level. Top left: pure functionals; top right: global hybrids with less than 30% of exact exchange; bottom left: other global hybrids; and bottom right: range-separated hybrids.

intense first band, whereas global hybrids including 40−60% of exact exchange as well as range-separated approaches relying on a relatively small damping parameter give the opposite trends: too short wavelengths but accurate intensities and topology. For these reasons, we have chosen to use five functionals in Section 3.4: the popular B3LYP and PBE0 that provide wavelengths on the experimental spot (573 and 543 nm, for the former) but incorrect relative intensities; M06-2X, a global hybrid including a large share of HF exchange, that overestimates the transition energy but gives a correct topology (see Supporting Information and ref 13); as well as CAM-B3LYP and ωB97XD, two range-separated hybrids providing an interesting compromise between wavelengths and intensities.

3.3. Analysis for 1,4-NH_2-AQ. Figure 3 compares the experimental and theoretical (ωB97XD) shapes of the visible band of **I** in cyclohexane. This figure also provides the main vibronic contributions through a stick spectrum. The agreement between the measured and the predicted topologies is obvious, though the selected functional locates the maximal absorption at 512.9, 508.8, and 479.8 nm and therefore undershoots the experimental wavelengths,[13] as already discussed in the previous section. However, the separation between the first and second (third) peaks attains 274 (1345) cm^{-1} with PCM-TD-ωB97XD, in very good match with the measurement 341 (1312) cm^{-1}, thus substantiating the predictive power of the selected approach. As expected, the first maximum principally originates from the 0−0 line. Although a blend of several vibrational modes contribute to the second and third peaks, one can mainly ascribe the bands to modes 14 (408 cm^{-1}) and 18 (479 cm^{-1}), 56 (1421 cm^{-1}) and 58 (1491 cm^{-1}) of the excited state, respectively (see Figure 3). Representations of these modes can be found in Supporting Information. Modes 14 and 18 correspond to bending of the amino groups and breathing of the aromatic ring bearing the two amines. On the other hand, the high-intensity band is related to stretchings of the same ring and displacements of the hydrogen atoms of the amines. Therefore, the substituents play a key role in the experimental shape, though the main coupling mode does not correspond to very intense IR C−N elongation (computed at an higher 1604 cm^{-1} for S_1) as historically proposed for amino-AQ.[24] We have also simulated the spectra of **I** in dioxane. Convoluting the spectrum with a 0.04 eV fwhm Gaussian, we obtain two maxima at 510 and 481 (579 and 543) nm with relative intensities of 0.89 and 1.00 (1.00 and 0.94) applying ωB97XD (B3LYP), and this nicely fits the relative experimental intensities (positions of the bands): 585 (0.92) and 547 (1.00) nm.[9]

For **I**, these results seem to confirm the experimental analysis[24] that the shape of the visible absorption band is related to vibronic interactions. Let us nevertheless assess the possibility to form "conventional" tautomers corresponding to the transfer of one or two protons between the carbonyl and the amine (Figure 4). Using ωB97XD, a functional accurate for electronic spectra, H-bond and other weak interactions,[83,87,88] we computed λ_{vert} of 467, 496, and 447 nm for the canonical structure, the tautomer corresponding to a first proton transfer between the amine and carbonyl groups and the double tautomer, respectively (see Figure 4). Such results may apparently fit the two peaks and shoulder topology found in polar environments.[9,86] However, by analyzing the relative energies of all species as well as the corresponding transition states, one clearly notes that the apparent agreement is purely fortuitous. Indeed, on the ground-state potential energy surface, the first proton transfer not only requires an energy more than 20 times the thermal energy (13.6 kcal·mol^{-1}) but also yields a product very close to the transition state. This implies that even if the transfer occurs (a very unlikely event), the back reaction will be instantaneous; the computed back reaction barrier is <0.05 kcal·mol^{-1}. For the second proton transfer, the situation is quite similar and leads to a very unstable product. Of course, one has also to probe the S_1 potential energy surface, as a more complex process (absorption of the canonical form, excited-state proton transfer, relaxation to the ground-state tautomer, and photon absorption of this tautomer) may also occur. To test this hypothesis, we have tried to optimize the S_1 geometries of both tautomers, but they systematically converged to the canonical form. This can be explained by examining Figure 4 that indicates that there is no minimum on the excited-state surface for the tautomers. Fain and co-workers have recently proposed that the multiple bands of **I** correspond to the presence of several more exotic species (see refs 22 and 23 as well as references therein) corresponding to tautomers of 4,9-diamino-1,10-anthraquinone (see central molecule in Figure 5), itself obtained by exchanging of one carbonyl and one amine in **I**. These authors did not propose a chemical path to obtain their structure (and there is, to the best of our knowledge, no experimental proof of their existence), but they justify this choice with the correlation between the λ_{max} computed with a semiempirical approach for the different tautomers and the measured positions for the maxima.[22] This 4,9-diamino-1,10-anthraquinone derivative is less stable than **I** by 6.3 kcal·mol^{-1} and presents a S_0 dipole moment of 1.7 D at the PCM-(cyclohexane)-ωB97XD/6-31++G(d,p) level. This value can

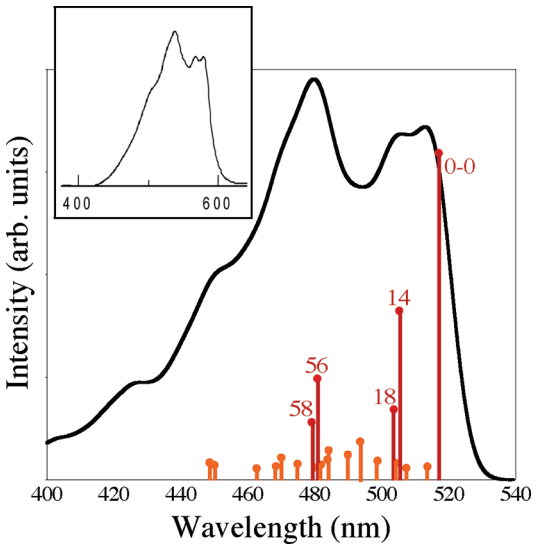

Figure 3. Computed ωB97XD spectra of **I**, using a convoluting Gaussian with fwhm 0.03 eV. The main contributions to the stick spectrum are shown, with numbers corresponding to the vibrational modes for the four largest contributions. The top panel is the experimental graph reprinted with permission from Khan, M. S. and Khan, Z. H. Electronic absorption spectra of amino-substituted anthraquinones and their interpretation using the ZINDO/S and AM1 methods. *Spectrochim. Acta, Part A* **2003**, *59*, 1409−1426. Copyright 2003, Elsevier.

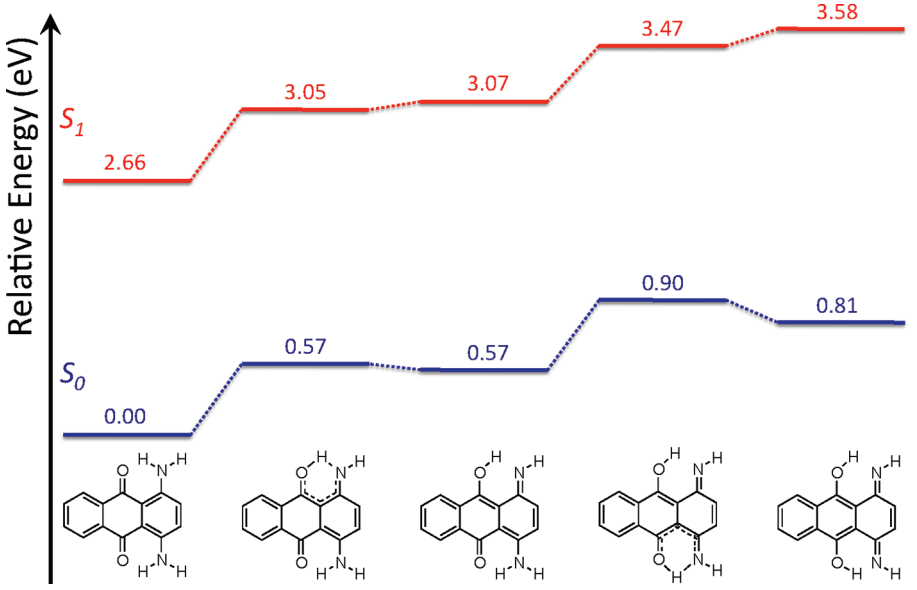

Figure 4. Representation of the relative total energies of the tautomers of **I** together with the transition states. All values are in eV. The S_1 energies are computed within the vertical approximation (PCM-(TD-)ωB97XD/6-31++G(d,p)). Representation of the imaginary modes characteristics of the transition states can be found in Supporting Information.

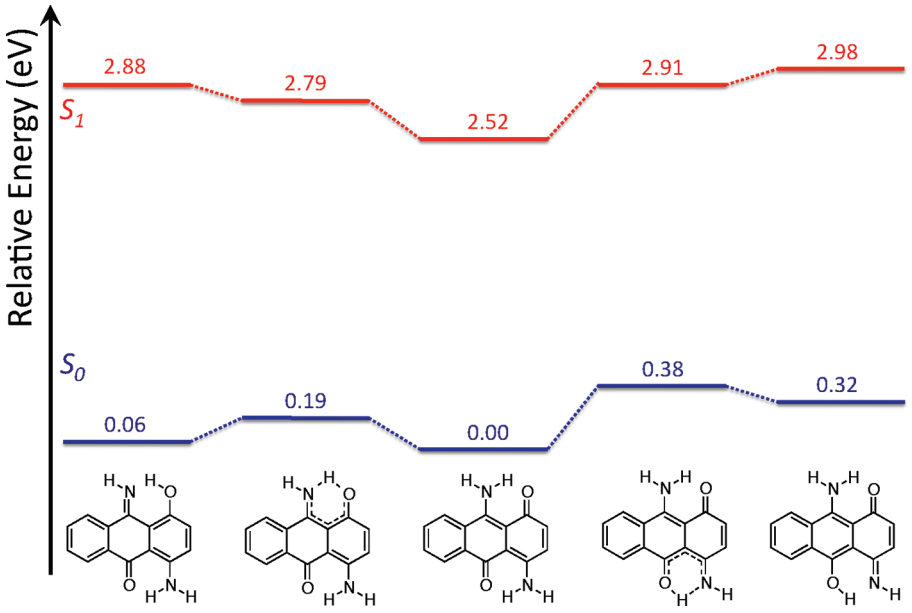

Figure 5. Representation of the relative total energies of the tautomers of 4,9-diamino-1,10-anthraquinone obtained at the PCM-(TD-)ωB97XD/6-31++G(d,p) level of theory.

be compared to the 3.6 D value obtained for **I**, with the same method and, to the 3.1 D figure obtained by the most recent experimental measurements.[89] Likewise, the excited-state dipole moment is estimated to be larger than its ground-state counterpart by 0.6−1.8 D (depending on the selected experimental method, see ref 89), and we compute a variation of −0.4 D for 4,9-diamino-1,10-anthraquinone and +2.3 D for 1,4-diamino-9,10-anthraquinone. Clearly, these values are not in favor of a significant contribution of the former "exotic" structure. Nevertheless, we have investigated its tautomers and the corresponding transition states (see Figure 5). First let us note that a stable "double" tautomer could not be located on the ground-state surface despite several attempts. It systematically reverts to one of the two possible "single" tautomeric forms, hinting that it is risky to attribute one band to such compound. For the most stable tautomer, we find a reaction barrier of 4.4 kcal·mol^{-1}. If one uses classical Boltzmann and transition-state theories, one obtains only 9% of this tautomer (that presents a smaller oscillator strength than both **I** and 4,9-diamino-1,10-anthraquinone) and a back reaction 10 times faster than the foward reaction. The second tautomer is too high in energy to impact significantly. In short, our analysis rules out any significant proportion of conventional or exotic tautomers in solution.

We have also tested the possible presence of aggregates in solution. For **I**, the only available XRD structure corresponds to a dihydrate with inter-AQ interactions mostly proceeding through water-assisted H-bonds.[84] In the course of defining reasonable starting points for our geometry optimizations, we have therefore decided to recrystallize **I**[90] and actually obtained a new XRD structure (see cif files and Supporting Information). This water-free structure has a completely different packing than the previously reported one, with AQ arranged in a slipped antiparallel orientation along the first axis, bonded through intermolecular H-bonds between the amine and the carbonyl for the second and displaying a weaker π−π stacking along the third direction. The data from both XRD structures as well as chemical intuition have been used to define the initial coordinates for our geometry optimizations of the dimers of **I**. We have reached four different structures that are represented in Supporting Information: two, **A** and **B** presents cofacial head-to-tail **I** with H-bonds between both carbonyl and amino groups, and two, **C** and **D**, are characterized by H-bonded side-by-side (but not coplanar) AQ. Their spectral features are listed in Table 3. At the PCM-ωB97XD/6-31++G(d,p) level, only the two first aggregates are characterized by a stabilizing interaction energy compared to the monomer: −3.51 kcal·mol^{-1} for **A** and −1.04 kcal·mol^{-1} for **B**. Their spectra display small bathochromic (**A**) and hypsochromic (**B**) shifts compared to the isolated case but only possess a major absorption band. In a naive view, one could imagine that the first experimental band at 578.4 nm corresponds to the most stable dimer, the 567.2 nm absorption to the monomer, and the most intense band 537.6 nm to the **B** dimer. However, with these assignments, the energetic separation between the first and the most intense band would be 0.11 eV, in poor agreement with experiment (0.16 eV) and with vibronic simulations (0.17 eV). Consistently with experimental investigations carried out for different concentration of dyes,[24] this analysis therefore hints that aggregation falls short to provide a convincing explanation to the experimental findings.

Table 3. Relative Free Energies (kcal·mol^{-1}) and Vertical Transition Wavelengths (nm) for Four Dimers of I[a]

		ΔG	λ_{max}
A	π−π + H-bond	0.00	474 (0.35)
B	π−π + H-bond	2.47	455 (0.51)
C	H-bonded	9.16	468 (0.51)
D	H-bonded	8.94	478 (0.52) and 469 (0.16)

[a] See Supporting Information. All calculations performed at the PCM-(TD-)ωB97XD/6-31++G(d,p) level.

3.4. The Dihydroxy Series. The results obtained with five functionals for three dihydroxy-AQ are listed in Table 4. Though

Table 4. Predicted Values in the Dihydroxy Series. [a]

		ground state					excited state					vibronic				
dye	functional	PG	$d_{C=O}$	d_{C-O}	d_{Hbond}	λ_{vert} (f)	ZPVE	PG	$d_{C=O}$	d_{C-O}	d_{Hbond}	λ_{vert} (f)	ZPVE	ΔG	P_1^{conv} (I_r)	P_2^{conv} (I_r)	P_3^{conv} (I_r)
II	B3LYP	C_{2v}	1.251	1.341	1.658	475 (0.22)	5.15	C_{2v}	1.264	1.330	1.573	551 (0.22)	5.06	2.32	531 (1.00)	495 (0.83)	464 (0.41)
	PBE0	C_{2v}	1.246	1.331	1.633	461 (0.24)	5.18	C_{2v}	1.259	1.319	1.535	535 (0.24)	5.10	2.38	516 (1.00)	482 (0.85)	453 (0.45)
	M06-2X	C_{2v}	1.236	1.338	1.715	401 (0.27)	5.20	C_{2v}	1.260	1.312	1.505	501 (0.28)	5.09	2.65	427 (1.00)		
	CAM-B3LYP	C_{2v}	1.241	1.337	1.666	413 (0.28)	5.22	C_{2v}	1.262	1.316	1.523	497 (0.28)	5.12	2.63	469 (0.73)	460 (0.74)	440 (1.00)
	ωB97XD	C_{2v}	1.240	1.336	1.690	409 (0.29)	5.22	C_{2v}	1.260	1.315	1.552	490 (0.28)	5.12	2.67	462 (0.74)	453 (0.76)	434 (1.00)
III	B3LYP	C_{2h}	1.249	1.341	1.669	438 (0.29)	5.15	C_s	1.274/1.268	1.341/1.317	1.636/1.456	514 (0.23)	5.03	2.54	477 (0.87)	455 (1.00)	
	PBE0	C_{2h}	1.243	1.331	1.643	420 (0.31)	5.20	C_s	1.271/1.262	1.330/1.305	1.602/1.385	499 (0.26)	5.06	2.62	461 (0.90)	440 (1.00)	
	M06-2X	C_{2h}	1.234	1.337	1.721	357 (0.38)	5.20	C_s	1.306/1.250	1.334/1.268	1.679/1.037	518 (0.35)	5.09	2.92			
	CAM-B3LYP	C_{2h}	1.239	1.336	1.674	371 (0.38)	5.22	C_s	1.309/1.256	1.334/1.272	1.633/1.035	521 (0.37)	5.12	2.91			
	ωB97XD	C_{2h}	1.237	1.335	1.700	367 (0.39)	5.22	C_s	1.274/1.259	1.332/1.302	1.637/1.403	439 (0.34)	5.07	3.00	405 (0.99)	386 (1.00)	
IV	B3LYP	C_{2v}	1.229/1.267	1.343	1.686	439 (0.29)	5.15	C_s	1.246/1.295	1.321/1.342	1.677/1.510	507 (0.23)	5.04	2.53	483 (0.94)	473 (0.94)	454 (1.00)
	PBE0	C_{2v}	1.223/1.261	1.333	1.665	421 (0.31)	5.20	C_s	1.240/1.291	1.310/1.331	1.649/1.469	487 (0.26)	5.08	2.62	464 (0.92)	456 (1.00)	437 (1.00)
	M06-2X	C_{2v}	1.218/1.250	1.338	1.729	362 (0.37)	5.20	C_s	1.233/1.298	1.299/1.331	1.686/1.387	441 (0.34)	5.05	2.94	383 (1.00)		
	CAM-B3LYP	C_{2v}	1.221/1.257	1.338	1.687	376 (0.37)	5.23	C_{2v}	1.238/1.298	1.318	1.541	433 (0.38)	5.08	2.92	413 (0.93)	395 (1.00)	
	ωB97XD	C_{2v}	1.220/1.254	1.336	1.707	373 (0.36)	5.22	C_{2v}	1.238/1.294	1.317	1.565	429 (0.38)	5.09	2.95	408 (0.96)	391 (1.00)	

[a] All calculation with the PCM(pentane)-(TD-)DFT/6-31++G(d,p) approach. The vibronic maxima have been obtained with a fwhm Gaussian of 0.05 eV. See caption of Table 1 for more details.

Figure 6. Comparison between the experimental and theoretical shapes for the visible absorption band of (from top to bottom) **II**−**IV** taking the first maximum as reference. The measured data have been extracted from ref 19 and recast on the energy scale, whereas theoretical values have been obtained at the PCM-TD-ωB97XD/6-31++G(d,p) level of theory, using a convoluting sum of Gaussian functions with a fwhm of 0.023 eV for all cases.

II−**IV** are all characterized by two H-bonds between carbonyl and alcohol groups, they differ by their symmetry. Recent experimental data in *n*-pentane show a significantly variations of the position for the characteristic visible band, each band possessing a specific vibronic signature.[19] The ZPVE computed with all functionals is similar for the three dyes and shows only a

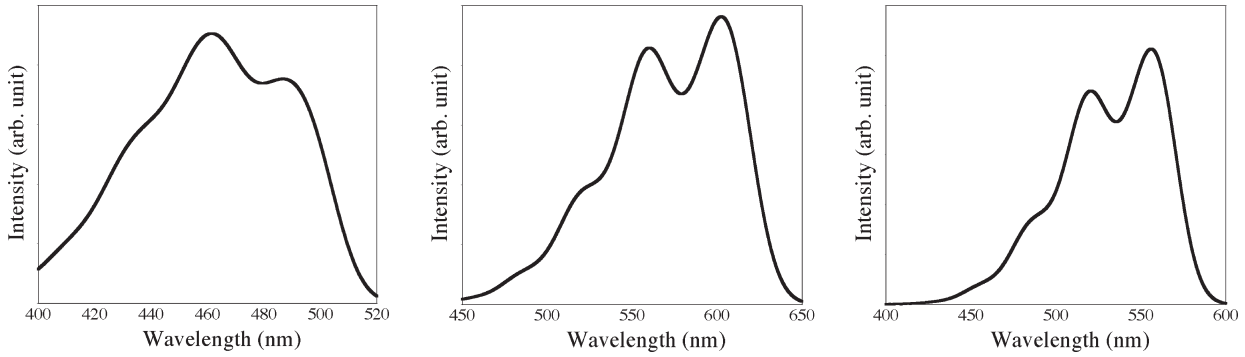

Figure 7. PCM-TD-ωB97XD/6-31++G(d,p) spectra computed for **V** (left, methanol), **VI** (central, ethanol), and **VII** (right, cyclohexane) using a convoluting sum of Gaussian functions with fwhm of 0.50 eV in all cases.

ca. −0.1 eV shift when going from the ground state to the excited state, confirming that the ZPVE variation may be rapidly estimated with any functional. As noted in Section 3.2, the predicted vertical wavelengths increase with the amount of *exact* exchange included in the hybrid.

For **II**, Table 4 shows the same trends as for its amino counterpart, **I**: photon absorption yields an extension of the carbonyls and a concomitant shortening of both the single C−O bonds and the H-bond intervals. Nevertheless, for the latter the variation accompanying the electronic transition is much more pronounced than in **I**, a phenomenon related to the symmetric/asymmetric nature of the H-bond. The vibronic spectra obtained with a fwhm of 0.03 eV are shown in Supporting Information, and they follow the same qualitative evolution as for **I** when modifying the functional. B3LYP and PBE0 not only provide a first absorption at 531 and 516 nm, respectively, the latter being on the experimental spot (517 nm),[19] but also predict a dominant 0−0 band, which is inconsistent with measurements.[19] In terms of shape, it turns out that the best theory/experiment match is reached with CAM-B3LYP or ωB97XD, as illustrated in Figure 6, but at the price of less accurate positions for the first band: 469 and 461 nm, respectively. This corresponds to a ca. 0.25 eV error, which is in the line of average TD-DFT accuracy but remains sizable for a well-behaved low-lying $\pi-\pi^*$ transition (see the Introduction Section for reference benchmarks). As can be seen in Figure 6, following the 0−0 band, one notices a second absorption of equal intensity at ca. 470 cm^{-1}, followed by a dominating band peaking at ca. 1440 cm^{-1}. The two main S_1 vibrational modes responsible for these vibronic effects are 16 (479 cm^{-1}) and 49 (1311 cm^{-1}), respectively. The first corresponds to an extension of the phenyl ring bearing the hydroxyl groups, whereas the second is related to stretching of the phenyl rings and bending of the hydrogen atoms of the alcohols (animations may be found in the Supporting Information).

For **III**, the ground-state carbonyl bonds are slightly shorter than for **II**, and the transition energies are larger, which agrees with experiment. The S_0 inversion symmetry is lost at the excited state and it is quite clear from Table 4 that one hydroxyl group is strongly affected transition. This is a marked difference with respect to **II** that presented the same kinds of intramolecular interactions in S_0 and S_1, indicating that the ground-state geometries and vertical transition energies may not provide a complete picture of the chemical differences between these two dyes. With B3LYP, PBE0 and ωB97XD, one H-bond of **III** is significantly shorten (ca. 0.25 Å) by photon absorption, whereas for M06-2X and CAM-B3LYP, the S_1 optimization actually yield to a tautomeric form, with one alcohol function at the center of the AQ. In other words, with these latter hybrids, the ground- and excited-state geometries are not simple variations, and it becomes obvious that a "conventional" approximation cannot be applied to calculate the vibrationally resolved band. Consequently, in the Supporting Information, we report the vibronic (stick and convoluted) spectra for B3LYP, PBE0, and ωB97XD only. The best qualitative agreement is again reached with ωB97XD (see Figure 6) with two maxima of nearly equal intensities. For **III**, theory reproduces the camel-back shape of the experimental spectrum, though the separation between the two maxima is clearly overshot by the model. We attribute this error to the application of an harmonic approximation that is obviously becoming less suitable for strongly distorted O−H bonds. Indeed, the most important coupling mode, responsible for the first extremum, corresponds to proton transfer between the two oxygen atoms, whereas the second maximum originates to a large panel of modes implying both alcohols. It is also worth noting that the first peak (406 nm) does not exactly correspond to the 0−0 band (413 nm), making comparisons between experimental and theoretical λ_{max} a nontrivial task.

For **IV**, the highest PG is only systematically conserved with the two range-separated functionals, all three global hybrids providing an asymmetric excited state, with one long and one short H-bond, although contrary to **III**, we found no clear-cut tautomer. Once again, B3LYP and PBE0 yield transition energies in good agreement with experiment with deviations of ca. 20 nm. No functional is fully satisfying in terms of shape (Figure 6 and Supporting Information), and as for **III**, this effect is related to anharmonicties as the O−H bond are strongly elongated for **IV** (see Table 4). This induces a too large separation in the stick spectrum (overestimates frequencies), and subsequently, a clear-cut minium in the convoluted spectrum that is not found in the experiment.

3.5. Application to Other AQ Dyes. We have used ωB97XD to compare the experimental and theoretical spectra of three dyes of industrial interest: quinalizarin (**V**) a tetra-hydroxy-AQ, disperse blue 14 (**VI**), and solvent blue 59 (**VII**), two amino-substituted AQ presenting large extinction coefficients. All three dyes present well-structured absorption bands,[7,9,91] the latter containing 40 atoms and represents a computational challenge at this level of theory. The simulated spectra can be found in Figure 7. For **V**, the spectrum measured in methanol is very broad and presents two maxima reported at 512 and 490 nm by Green[7] and at 517 and 495 nm by Perkampus.[9] The simulation provides 486 and 462 nm, a 0.13 eV separation

that apparently fits experiment (0.11 eV) though we do not obtain exactly the same topology. The computed spectra of **VI** and **VII** are similar, and this outcome fits experiment.[7,91] For **VII**, one can estimate the experimental wavelengths (relative intensities) to be 643 nm (1.00), 600 nm (0.84), and 560 nm (sh, 0.39) in cyclohexane,[91] whereas TD-DFT yields 556 nm (1.00), 521 nm (0.83), and 490 nm (sh, 0.35), in obvious qualitative agreement but for the too large transition energies. Nevertheless, the shift of the main band compared to **I** in the same solvent is −0.19 eV in theory and −0.22 eV in the experiment, illustrating the accuracy of auxochromic displacements. Note that there is also an inversion of relative intensities of the two first peaks compared to **I**, and this effect is perfectly reproduced by ωB97XD. For disperse blue 14, experiment yields 640 nm (1.00), 594 nm (0.83), and 550 nm (sh, 0.43) in methanol,[7] whereas TD-DFT gives: 603 nm (1.00), 560 nm (0.89), and 522 nm (sh, 0.41), again in good qualitative agreement. As the solvent used for this latter AQ is polar and protic, the auxchromic displacement wrt **I** and **VII** cannot be compared directly due to the application of a continuum model.

4. CONCLUSIONS

We have computed vibrationally resolved absorption spectra of a series of amino and hydroxy anthraquinone dyes, using a time-dependent density functional approach accounting for bulk environmental effects. It turned out that the selected atomic basis set has a relatively modest impact on the properties, provided polarization functions are used. On the contrary, the selected DFT functional strongly affects the computed transition wavelengths, the geometries as well as the topology of the vibronic envelope, although it does not modify significantly the ZPVE energy differences computed for the ground and excited states. As no functional delivers fully consistent values, pinpointing the most adequate approach is not straightforward. Nevertheless, one can discard both pure functionals and hybrids including a very large share of exact exchange. In the present case, B3LYP and PBE0 provide accurate positions (wavelengths) for the absorption peaks but are less efficient than two range-separated hybrids, namely CAM-B3LYP and ωB97XD, to determine the shapes of the absorption bands (that is relative intensities). For 1,4-NH_2-AQ, our calculations show that the experimental spectrum cannot be easily explained by the presence of tautomers nor aggregates, but that it results from four major coupling modes implying the amino groups. For 1,4-OH-AQ, 1,4-NHMe-AQ, and 1,4-NHEt-AQ, the agreement between simulated and measured electronic spectra is also rather astonishing. This is an essential fact, as most AQ industrial dyes used today rely on a 1,4 pattern with strong H-bond donors. On the contrary, for 1,5-OH-AQ and 1,8-OH-AQ, the positions of the hydrogen atoms implied in intramolecular H-bonds are strongly modified following photon absorption, and the theory/experiment match is less satisfying. This is probably related to the harmonic approximation that becomes nonsuitable to evaluate vibrations related to distorted bonds. Therefore, efforts to include anharmonicity are of primary importance to further improve the description of the visible bands of hydroxy-AQ. Besides, this work illustrates the limitations of the available functionals and the developments that are still necessary to obtain new approaches able to correctly restore the experimental features typical of electronically excited states.

■ ASSOCIATED CONTENT

Supporting Information. Representation of all stick spectra for the benchmark study of **I**, these graphs use a Gaussian with a fwhm of 0.03 eV. Four principal vibrational modes of **I** related to Figure 3. Movies of the imaginary modes for the TS of Figures 4 and 5. Description of the XRD structure and cif file, deposited at the Cambridge Crystallographic Data Centre under number CCDC 819514. Representation of optimized dimers. Representation of all stick spectra for **II**−**IV** convoluted using a Gaussian with a fwhm of 0.03 eV. This material is available free of charge via the Internet at http://pubs.acs.org.

■ AUTHOR INFORMATION

Corresponding Author

*E-mail: denis.jacquemin@univ-nantes.fr; carlo-adamo@chimie-paristech.fr.

■ ACKNOWLEDGMENT

The authors thank Dr. C. Peltier (Paris) and Dr. J. Ceron (Nantes) for fruitful discussions and their help. D.J. is indebted to the Région des Pays de la Loire for financial support in the framework of a recrutement sur poste stratégique. The authors are indebted to the COST program CODECS and its members for support and many helpful discussions, respectively. This research used resources of: (1) the Interuniversity Scientific Computing Facility located at the University of Namur, Belgium, which is supported by the F.R.S.-FNRS under convention no. 2.4617.07; (2) the GENCI-CINES/IDRIS (grant c2011085117); and (3) the CCIPL (Centre de Calcul Intensif des Pays de Loire).

■ REFERENCES

(1) Iwanaga, H.; Aiga, F. *Liq. Cryst.* **2011**, *38*, 135–148.
(2) Palaniappan, S.; Manisankar, P. J. *Polym. Res.* **2011**, *18*, 311–317.
(3) Werner, S. J.; Linz, G. M.; Carlson, J. C.; Pettit, S. E.; Tupper, S. K.; Santer, M. M. *Appl. Anim. Behav. Sci.* **2011**, *129*, 162–169.
(4) Zhang, J.; Redman, N.; Litke, A. P.; Zeng, J.; Zhan, J.; Chan, K. Y.; Chang, C.-W. T. *Bioorg. Med. Chem.* **2011**, *19*, 498–503.
(5) Labhart, H. *Helv. Chim. Acta* **1957**, *40*, 1410–1421.
(6) Griffiths, J. *Colour and Constitution of Organic Molecules*; Academic Press: London, 1976.
(7) Green, F. J. *The Sigma-Aldrich Handbook of Stains, Dyes and Indicators*; Aldrich Chemical Company, Inc: Milwaukee, WI, 1990.
(8) Christie, R. M. *Colour Chemistry*; The Royal Society of Chemistry: Cambridge, U.K., 1991; p 228.
(9) Perkampus, H. H. *UV/Vis. Atlas of Organic Compounds*, 2nd ed.; VCH: Weinheim, Germany, 1992.
(10) Hunger, K. *Industrial Dyes*; Wiley-VCH: Weinheim, Germany, 2003.
(11) Fabian, J.; Hartmann, H. *Light Absorption of Organic Colorants*; Springer-Verlag: Berlin, Germany, 1980; Vol. 12 of Reactivity and Structure Concepts in Organic Chemistry.
(12) Zollinger, H. *Color Chemistry, Syntheses, Properties and Applications of Organic Dyes and Pigments*, 3rd ed.; Wiley-VCH: Weinheim, Germany, 2003; p 647.
(13) Khan, M. S.; Khan, Z. H. *Spectrochim. Acta A* **2003**, *59*, 1409–1426.
(14) Dahiya, P.; Choudhury, S. D.; Maity, D. K.; Mukherjee, T.; Pal, H. *Spectrochim. Acta A* **2008**, *69*, 134–141.
(15) Siddlingeshwar, B.; Hanagodimath, S. M. *Spectrochim. Acta A* **2009**, *72*, 490–495.
(16) Yoon, C.; Choi, J.-H.; Kim, J. P. *Mol. Cryst. Liq. Cryst.* **2010**, *533*, 102–112.

(17) Jung, J.; Park, Y.; Jaung, J.-Y.; Park, J. *Mol. Cryst. Liq. Cryst.* **2010**, *529*, 88–94.
(18) Sezer, B.; Sener, M. K.; Koca, A.; Erdogmus, A.; Avciata, U. *Synth. Met.* **2010**, *160*, 2155–2166.
(19) Khan, M. S.; Khan, Z. H. *Can. J. Anal. Sci. Spectrosc.* **2002**, *47*, 146–156.
(20) Giles, C. H.; Shah, C. D. *Trans. Faraday Soc.* **1969**, *65*, 2508–2515.
(21) Wegerle, D. J. Soc. *Dyers Colour* **1973**, *89*, 54–55.
(22) Fain, V. Y.; Zaitsev, B. E.; Ryabov, M. A. *Russ. J. Org. Chem.* **2009**, *45*, 374–382.
(23) Fain, V. Y.; Zaitsev, B. E.; Ryabov, M. A.; Strashnov, P. V. *Russ. J. Gen. Chem.* **2010**, *80*, 1986–1995.
(24) Sinclair, R. S.; Mc Alpine, E. *J. Soc. Dyers Colour* **1975**, *91*, 399–405.
(25) Jacquemin, D.; Peltier, C.; Ciofini, I. *Chem. Phys. Lett.* **2010**, *493*, 67–71.
(26) Guillaumont, D.; Nakamura, S. *Dyes Pigm.* **2000**, *46*, 85–92.
(27) Jacquemin, D.; André, J. M.; Perpète, E. A. *J. Chem. Phys.* **2004**, *121*, 4389–4396.
(28) Perpète, E. A.; Wathelet, V.; Preat, J.; Lambert, C.; Jacquemin, D. *J. Chem. Theory Comput.* **2006**, *2*, 434–440.
(29) Jacquemin, D.; Wathelet, V.; Preat, J.; Perpète, E. A. *Spectrochim. Acta A* **2007**, *67*, 334–341.
(30) Matsuura, M.; Sato, H.; Sotoyama, W.; Takahashi, A.; Sakurai, M. *J. Mol. Struct. (THEOCHEM)* **2008**, *860*, 119–127.
(31) Jacquemin, D.; Perpète, E. A.; Scuseria, G. E.; Ciofini, I.; Adamo, C. *J. Chem. Theory Comput.* **2008**, *4*, 123–135.
(32) Jacquemin, D.; Wathelet, V.; Perpète, E. A.; Adamo, C. *J. Chem. Theory Comput.* **2009**, *5*, 2420–2435.
(33) Jacquemin, D.; Perpète, E. A.; Ciofini, I.; Adamo, C.; Valero, R.; Zhao, Y.; Truhlar, D. G. *J. Chem. Theory Comput.* **2010**, *6*, 2071–2085.
(34) Foresman, J. B.; Head-Gordon, M.; Pople, J. A.; Frisch, M. J. *J. Phys. Chem.* **1992**, *96*, 135–149.
(35) Guido, C. A.; Mennucci, B.; Jacquemin, D.; Adamo, C. *Phys. Chem. Chem. Phys.* **2010**, *12*, 8016–8023.
(36) Jacquemin, D.; Perpète, E. A.; Assfeld, X.; Scalmani, G.; Frisch, M. J.; Adamo, C. *Chem. Phys. Lett.* **2007**, *438*, 208–212.
(37) van Caillie, C.; Amos, R. D. *Chem. Phys. Lett.* **1999**, *308*, 249–255.
(38) Furche, F.; Ahlrichs, R. *J. Chem. Phys.* **2002**, *117*, 7433–7447.
(39) Dierksen, M.; Grimme, S. *J. Phys. Chem. A* **2004**, *108*, 10225–10237.
(40) Scalmani, G.; Frisch, M. J.; Mennucci, B.; Tomasi, J.; Cammi, R.; Barone, V. *J. Chem. Phys.* **2006**, *124*, 094107.
(41) Tomasi, J.; Mennucci, B.; Cammi, R. *Chem. Rev.* **2005**, *105*, 2999–3094.
(42) Santoro, F.; Improta, R.; Lami, A.; Bloino, J.; Barone, V. *J. Chem. Phys.* **2007**, *126*, 084509.
(43) Improta, R.; Scalmani, G.; Frisch, M. J.; Barone, V. *J. Chem. Phys.* **2007**, *127*, 074504.
(44) Santoro, F.; Improta, R.; Lami, A.; Bloino, J.; Barone, V. *J. Chem. Phys.* **2007**, *126*, 184102.
(45) Santoro, F.; Lami, A.; Improta, R.; Bloino, J.; Barone, V. *J. Chem. Phys.* **2008**, *128*, 224311.
(46) Improta, R.; Santoro, F.; Barone, V.; Lami, A. *J. Phys. Chem. A* **2009**, *113*, 15346–15354.
(47) Peltier, C.; Laine, P. P.; Scalmani, G.; Frisch, M. J.; Adarno, C.; Ciofini, I. *J. Mol. Struct. (THEOCHEM)* **2009**, *914*, 94–99.
(48) Jacquemin, D.; Peltier, C.; Ciofini, I. *J. Phys. Chem. A* **2010**, *114*, 9579–9582.
(49) Klaumuenzer, B.; Kroener, D.; Saalfrank, P. *J. Phys. Chem. B* **2010**, *114*, 10826–10834.
(50) Jacquemin, D.; Perpete, E. A.; Scalmani, G.; Ciofini, I.; Peltier, C.; Adamo, C. *Chem. Phys.* **2010**, *372*, 61–66.
(51) Friedländer, P. *Ber. Dtsch. Chem. Ges.* **1909**, *42*, 765–770.
(52) Slater, J. C. *Quantum Theory of Molecular ans Solids*; McGraw-Hill: New York, 1974; Vol. 4.
(53) Vosko, S. J.; Wilk, L.; Nusair, M. *Can. J. Phys.* **1980**, *58*, 1200–1211.
(54) Becke, A. D. *Phys. Rev. A* **1988**, *38*, 3098–3100.
(55) Lee, C.; Yang, W.; Parr, R. G. *Phys. Rev. B* **1988**, *37*, 785–789.
(56) Perdew, J. P.; Burke, K.; Ernzerhof, M. *Phys. Rev. Lett.* **1996**, *77*, 3865–3868.
(57) Boese, A. D.; Handy, N. C. *J. Chem. Phys.* **2002**, *116*, 9559–9569.
(58) Baker, J.; Pulay, P. *J. Chem. Phys.* **2002**, *117*, 1441–1449.
(59) Becke, A. D. *J. Chem. Phys.* **1993**, *98*, 5648–5652.
(60) Stephens, P. J.; Devlin, F. J.; Chabalowski, C. F.; Frisch, M. J. *J. Phys. Chem.* **1994**, *98*, 11623–11627.
(61) Xu, X.; Goddard, W. A., III *Proc. Natl. Acad. Sci. U.S.A.* **2004**, *101*, 2673–2677.
(62) Adamo, C.; Barone, V. *J. Chem. Phys.* **1999**, *110*, 6158–6170.
(63) Ernzerhof, M.; Scuseria, G. E. *J. Chem. Phys.* **1999**, *110*, 5029–5036.
(64) Zhao, Y.; Truhlar, D. G. *Theor. Chem. Acc.* **2008**, *120*, 215–241.
(65) Boese, A. D.; Martin, J. M. L. *J. Chem. Phys.* **2004**, *121*, 3405–3416.
(66) Becke, A. D. *J. Chem. Phys.* **1993**, *98*, 1372–1377.
(67) Zhao, Y.; Truhlar, D. G. *J. Phys. Chem. A* **2006**, *110*, 5121–5129.
(68) Yanai, T.; Tew, D. P.; Handy, N. C. *Chem. Phys. Lett.* **2004**, *393*, 51–56.
(69) Tawada, T.; Tsuneda, T.; Yanagisawa, S.; Yanai, T.; Hirao, K. *J. Chem. Phys.* **2004**, *120*, 8425–8433.
(70) Iikura, H.; Tsuneda, T.; Yanai, T.; Hirao, K. *J. Chem. Phys.* **2001**, *115*, 3540–3544.
(71) Chai, J. D.; Head-Gordon, M. *J. Chem. Phys.* **2008**, *128*, 084106.
(72) Chai, J. D.; Head-Gordon, M. *Phys. Chem. Chem. Phys.* **2008**, *10*, 6615–6620.
(73) Jensen, F. *Chem. Phys. Lett.* **2005**, *402*, 510–513.
(74) Note that the vertical transitions reported in Table 1 have been determined using a nonequilibrium PCM model for the ground state and an equilibrium PCM approach for the excited state. The latter cannot therefore be starightfowardly compared to fluorescence wavelengths, but this is not the focus of the present contribution.
(75) Jacquemin, D.; Perpète, E. A.; Vydrov, O. A.; Scuseria, G. E.; Adamo, C. *J. Chem. Phys.* **2007**, *127*, 094102.
(76) Peach, M. J. G.; Benfield, P.; Helgaker, T.; Tozer, D. J. *J. Chem. Phys.* **2008**, *128*, 044118.
(77) Silva-Junior, M. R.; Schreiber, M.; Sauer, S. P. A.; Thiel, W. *J. Chem. Phys.* **2008**, *129*, 104103.
(78) Goerigk, L.; Moellmann, J.; Grimme, S. *Phys. Chem. Chem. Phys.* **2009**, *11*, 4611–4620.
(79) Caricato, M.; Trucks, G. W.; Frisch, M. J.; Wiberg, K. B. *J. Chem. Theory Comput.* **2010**, *6*, 370–383.
(80) Jacquemin, D.; Perpète, E. A.; Ciofini, I.; Adamo, C. *J. Chem. Theory Comput.* **2010**, *6*, 1532–1537.
(81) Fabian, J. *Dyes Pigm.* **2010**, *84*, 36–53.
(82) Goerigk, L.; Grimme, S. J. *Chem. Phys.* **2010**, *132*, 184103.
(83) Jacquemin, D.; Perpète, E. A.; Ciofini, I.; Adamo, C. *Theor. Chem. Acc.* **2011**, *128*, 127–136.
(84) Kahino, S.; K., S.; Haisa, M. *Acta Cryst. C* **1988**, *44*, 1044–1046.
(85) Jacquemin, D.; Perpète, E. A.; Scuseria, G. E.; Ciofini, I.; Adamo, C. *Chem. Phys. Lett.* **2008**, *465*, 226–229.
(86) Weast, R. C. *Handbook of Chemistry and Physics*, 60th ed.; The Chemical Rubber Company: Cleveland, OH, 1979.
(87) Thanthiriwatte, K. S.; Hohenstein, E. G.; Burns, L. A.; Sherrill, C. D. *J. Chem. Theory Comput.* **2011**, *7*, 88–96.
(88) Burns, L. A.; Vazquez-Mayagoitia, A.; Sumpter, B. G.; Sherrill, C. D. *J. Chem. Phys.* **2011**, *134*, 084107.
(89) Siddlingeshwar, B.; Hanagodimath, S. M. *Spectrochim. Acta A* **2010**, *75*, 1203–1210.
(90) Crystals grown by slow diffusion of cylohexane into a solution of 1,4-diaminoanthraquinone in dichloromethane.
(91) Zakerhamidi, M. S.; Ghanadzadeh, A.; Moghadam, M. *Spectrochim. Acta A* **2011**, *79*, 74–81.